Applied Physics B (2025) 131:157
https://doi.org/10.1007/s00340-025-08482-3

Applied Physics B
Lasers and Optics

RESEARCH

Measurement of optical absorption in granular aluminum thin films at room temperature

Mario De Lucia[1,2] · Mahya Khorramshahi[3] · Thomas Reisinger[3] · Ioan Pop[3,4,5] · Gerhard Ulbricht[6,7]

Received: 16 December 2024 / Accepted: 4 May 2025 / Published online: 11 July 2025

Abstract

Because of their versatility and scalability, Microwave Kinetic Inductance Detectors (MKIDs) represent a rapidly developing class of cryogenic superconducting detectors. In the context of optical photon detectors, the efficiency of MKIDs faces limitations due to the reflection of visible and near-infrared (VIS-NIR) photons by low resistivity metallic films, which prevents a significant portion of incident photons from being absorbed and detected. To address this issue, we propose the use of granular Aluminum (grAl), a disordered superconductor which can achieve resistivity as high as 10 mΩ·cm. We measure optical transmission and reflection of grAl thin films in the wavelength range 400 nm to 1100 nm, from which we infer their absorption. Compared to other commonly used superconductors in the MKIDs community, for grAl we observe comparable or superior absorption, depending on the wavelength and the film thickness, which makes it a promising alternative material.

1 Introduction

Microwave Kinetic Inductance Detectors (MKIDs) are a class of superconducting cryogenic pair-breaking detectors with a plethora of applications in advanced instrumentation [1]. In particular, for optical and near-infrared astronomy, instruments such as ARCONS [2], DARKNESS [3] and MEC [4] have been demonstrated and deployed on sky. While these instruments clearly show that the state-of-the-art is well advanced, in the optical and near-infrared range further research and development can be beneficial in order to further improve detector performance. The optical properties of thin superconducting films are being widely investigated by the MKIDs community. Studies show promising results for TiN [5–7], Ti/TiN multilayers [5], Hf [8], β-Ta [7] and PtSi [6, 9].

Granular Aluminum (grAl) is a superconductor with a long standing record of scientific publications starting with Cohen and Abeles [10] in 1968. It is made up of nanometer-sized grains of superconducting Aluminum (Al) [11] coupled to each other through thin insulating layers of non-stoichiometric Aluminum Oxide (AlO_x) to form an effective 3-dimensional network of Josephson junctions [12]. Its superconducting properties, such as kinetic inductance and critical temperature, as well as the optical properties related to the film resistivity, can be tuned by varying the oxidation parameters during deposition. Remarkably, grAl can show superconductivity for relatively high resistivity up to 10 mΩ·cm [13], which corresponds to low reflectivity thin

✉ Mario De Lucia
mario.delucia@unipi.it

Mahya Khorramshahi
mahya.khorramshahi@kit.edu

Thomas Reisinger
thomas.reisinger@kit.edu

Ioan Pop
ioan.pop@kit.edu

Gerhard Ulbricht
ulbrichtg@cp.dias.ie

[1] Dipartimento di Fisica, Università di Pisa, Largo Bruno Pontecorvo 3, 56127 Pisa, Italy

[2] INFN - Pisa, Largo Bruno Pontecorvo 3, 56127 Pisa, Italy

[3] IQMT, Karlsruhe Institute of Technology, 76131 Karlsruhe, Germany

[4] PHI, Karlsruhe Institute of Technology, 76131 Karlsruhe, Germany

[5] Physics Institute I, Stuttgart University, 70569 Stuttgart, Germany

[6] Physics Department, Maynooth University, Maynooth, Ireland

[7] Astronomy and Astrophysics, Dublin Institute for Advanced Studies, Dublin 2 D02XF86, Ireland

films, promising for photon detectors. Superconducting grAl resonators and devices with relatively high internal quality factors $Q_i \approx 100,000$ have already been demonstrated [14–20], and used to implement kinetic inductance detectors for GHz [21] and THz [22] radiation.

Here we assess the possibility of using grAl for optical and near-infrared astronomy by investigating the absorption of grAl films for photons in the 400 nm - 1100 nm range. On visual inspection, grAl looks dark-grey and possibly exhibits higher absorption than more traditional superconductors in the same wavelength range. Possible advantageous features of optical grAl detectors for VIS-NIR MKIDs include small reflectivity [23], a high sheet-inductance which yields small pixel size and enables up-scaling the density of pixels on the focal plane of an instrument, a technically less involved thermal deposition method which does not require ultra-high vacuum, as well as a resilience to magnetic fields of up to 1 T [24]. It is also worth mentioning that the quasiparticle relaxation time for grAl films can be in excess of 1 s [16] in principle allowing for a long signal integration time. Previous optical characterisation of grAl films have focused on different morphologies with larger grains by one order of magnitude [23], obtained by thermal treatment at temperatures above 300 °C.

The grAl films discussed in this article were deposited at room temperature on c-plane Sapphire substrates by evaporation in an atmosphere with a partial pressure of oxygen. They are all nominally 20 nm thick and are uniform within 10% across the radius. Such uniformity is achieved by rotating the sapphire substrate around its axis during the evaporation process. These films exhibit resistivity values which are about one order of magnitude below the grAl superconducting-insulator transition, as summarized in Table 1 [25].

2 Optical transmittance

The optical transmittance of a sample is defined as the fraction of the incident optical flux that is not absorbed nor reflected by the sample. This is a measure of how transparent a certain sample is to incident radiation.

The experimental setup used to measure transmittance is shown in Fig. 1 and is composed of a broad-spectrum tungsten lamp filtered by a Quantum Design MSH-150 monochromator. The monochromatic light is coupled into an optical fiber, which is then connected to one of the four ports of an integrating sphere (Newport 819C) to uniformly illuminate the samples. This custom setup acts as a home-built spectrophotometer.

Table 1 GrAl films resistance and resistivity values obtained from a 4-probe measurement at room temperature, with a ±10% uncertainty. All films are nominally 20 nm thick

Sample	1	2	3	4	5
R(Ω/□)	1250	1000	550	220	170
$\rho(\mu\Omega\cdot\text{cm})$	2500	2000	1100	440	340

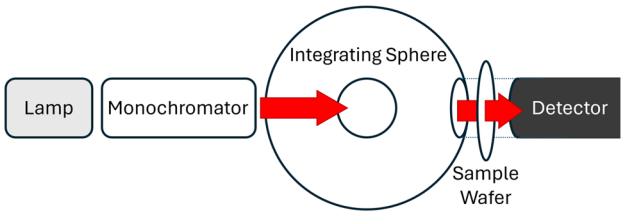

Fig. 1 Schematic of the experimental setup used for the thin film optical transmittance measurements. The light produced by the lamp is passed through a monochromator which scans the source from 400 nm to 1100 nm. The light is then shone through an integrating sphere and then through the sample into a photodiode in order to obtain a spectrum

The samples to be characterized are attached to a holder located at the second port, at 90° with respect to the first one. Behind the holder, we mounted a calibrated photo-diode (Thorlabs S120C) in order to measure the amount of light that is transmitted through the sample. The remaining two ports were kept closed with their caps. The whole setup is then placed inside a light-tight enclosure to avoid the effects of stray light.

The Transmittance $T_i(\lambda)$, presented in Fig. 2, is calculated for wavelengths λ between 400 nm and 1100 nm by computing the ratio

$$T_i(\lambda) = \frac{\text{grAl}_i(\lambda)}{\text{Sapphire}(\lambda)}, \tag{1}$$

where $grAl_i$ is the optical flux (after dark current subtraction) measured by the detector for the i-th sample and $Sapphire(\lambda)$ is the detected optical flux for a blank sapphire wafer. Here, we have neglected any second-order effects, such as those induced by multiple reflections at the interfaces. This approximation is justified by the small thickness of the film as described in Ballester et al. [26].

The error bars in Fig. 2 were determined by propagating the detector uncertainty: we measured a set of dark current values from which we calculated the standard deviation σ. We have then calculated the relative error for the optical flux values using 2σ and propagated it (See Appendix A.1). Note, that the sharp increase in noise around 800 nm is due to a change in the grating of the monochromator which results in a significant reduction of light passing it. The noise at the far ends of the spectrum are due to low intensity emitted from the monochromator in these wavelength ranges.

For samples 1 to 4, at a fixed wavelength (e.g. 1100 nm) the transmittance increases with increasing resistivity of the

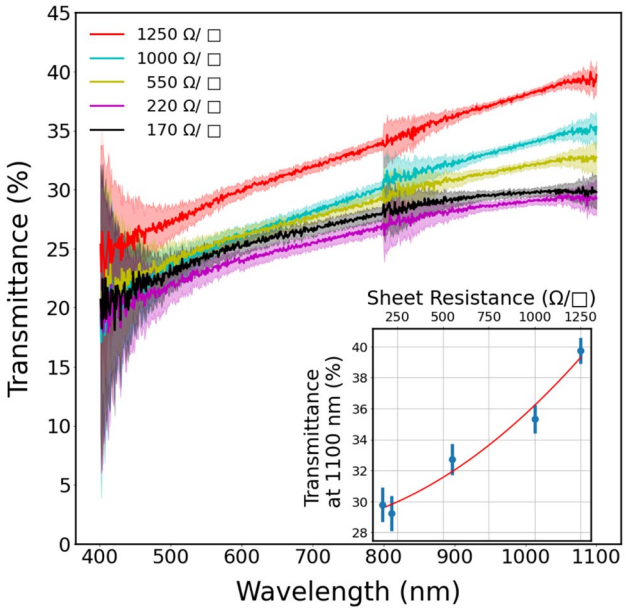

Fig. 2 Transmittance vs. wavelength for all grAl samples (see Table 1) measured using the setup in Fig. 1. Each colour corresponds to a different sheet resistance, according to the legend. The shaded areas represent the uncertainty on the measurements. The inset shows the measured transmittance at 1100 nm vs. the sheet resistance of the grAl film. The red line shows a quadratic fit to the data to guide the eye

film. For samples 5 and 6 (Black and magenta curves), we see that the trend seems reversed but still consistent within measurement uncertainties. This could be due to a sample mix-up, a drift in the lamp intensity or a drift in the detector efficiency.

The inset of Fig. 2 indicates a non-linear dependence of the transmittance as a function of the resistivity for different films.

3 Optical reflectance

The experimental setup shown in Fig. 3 consists of a broad-spectrum tungsten lamp connected to a Quantum Design MSH-150 monochromator the output of which is coupled to a fiber. The fiber is mounted at one end of a black plastic tube which is part of a light-tight box. At the other end of the tube, we place our samples, i.e., either a calibrated Al mirror (PF20-03-G01 from Thorlabs), a blank sapphire wafer, or the Sapphire + grAl film. We use a black cardboard behind the sample to reduce any spurious reflections. The light is reflected from the samples and then coupled into another optical fiber, mounted parallel to the first one. The collected light signal is then measured with the use of a calibrated photodiode (Thorlabs S120C). The setup is shielded inside a light-tight enclosure.

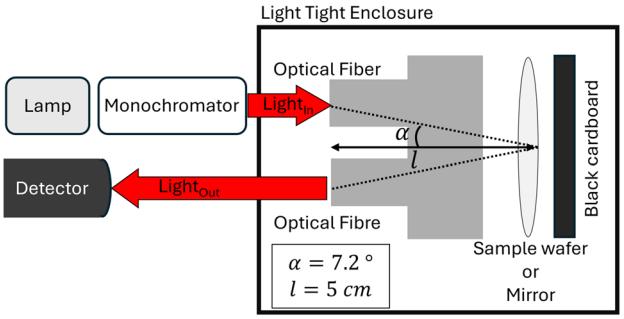

Fig. 3 Schematic of the experimental setup used for the thin film optical reflectance measurements. The gray shape represents the two fiber ends mounted at one extremity of the plastic tube

Following the scheme and the labels of Fig. 3, geometrical considerations allow us to set an upper limit for the angular deviation from perpendicular incidence:

$$\alpha = arctg\left(\frac{d_{\mathrm{SMA}}}{l}\right) = 7.2° \pm 0.5°,$$

where $d_{SMA} = 7.9$ mm is the diameter of the sub miniature A (SMA) connectors, which is also the distance between two fiber-core centers, and $l = 5$ cm. While the setup does not test the reflectivity at perpendicular incidence ($\alpha > 0$), it is important to note that α is far from Brewster's angle which varies with the refractive index of the sample between 60° and 65°, so the reflectance is expected to vary slowly with the angle of incidence.

In this configuration, the reflectance of the grAl films is given by the ratio between the signal read out by the detector when the Sapphire + grAl wafer is mounted in the sample space (taking into account its reflectivity) and the signal measured when the mirror is mounted re-normalized through the known reflectivity of the mirror itself. A thorough description of the measurement strategy can be found in Appendix B.1 We observe that the reflectance decreases as the film's resistivity increases at a fixed wavelength. The inset of Fig. 4 shows the reflectance of the grAl films at 1100 nm as a function of the resistivity of the films. The error bars in Fig. 4 were calculated following a similar recipe as described in the previous section, i.e. by evaluating the relative error of the detection and propagating it (for details see Appendix B.2).

Note, that the signal that reaches the detector in all cases is about one order of magnitude bigger than the previous case, hence the effects of the reduction of the throughput of the monochromator are not as relevant. For this reason, the nominal relative error on the measurement as provided by the manufacturer of the detector is greater than the contribution of the dark current, hence we used that for propagation. *Thorlabs* quotes 3% between 440 nm and 980 nm, 5%

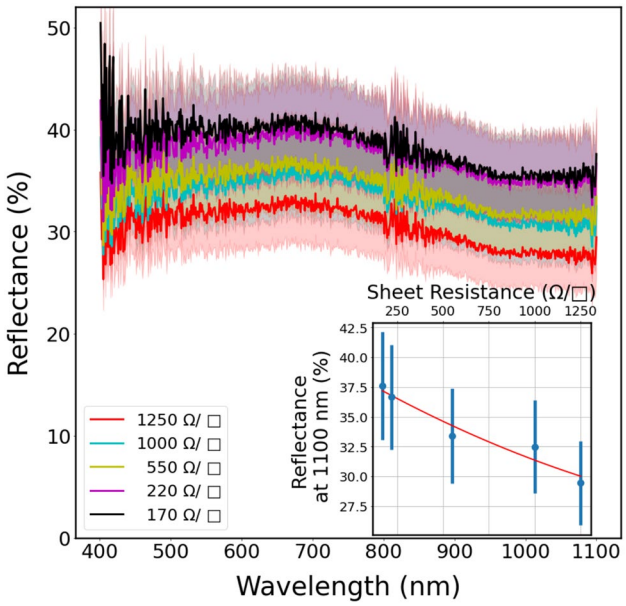

Fig. 4 Reflectance vs. wavelength for all grAl samples (see Table 1) measured using the setup in Fig. 3. Each colour corresponds to a different sheet resistance, according to the legend. The shaded areas represent the uncertainty of the measurements. The inset shows the measured reflectance at 1100 nm vs. the sheet resistance of the grAl film. The red line shows a quadratic fit to the data to guide the eye

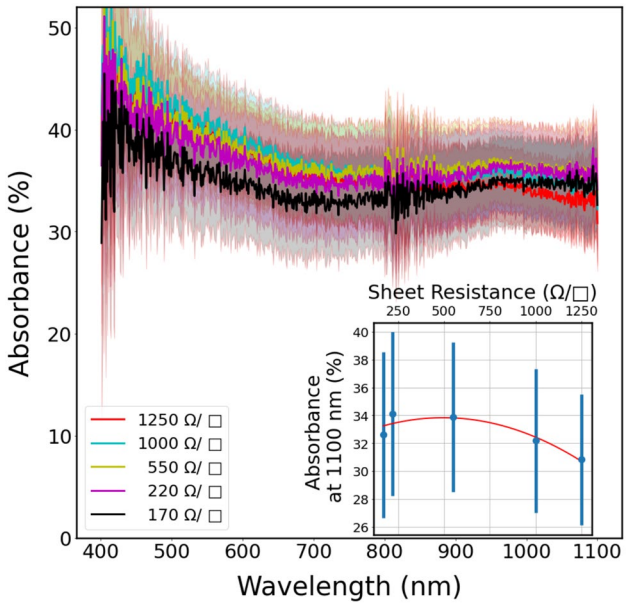

Fig. 5 Absorbance vs. wavelength for all grAl samples (see Table 1) obtained using Eq. 2. Each colour corresponds to a different sheet resistance, according to the legend. The shaded areas represent the uncertainty of the measurements. The inset shows absorbance at 1100 nm vs. the sheet resistance of the grAl film. The red line shows a quadratic fit to the data to guide the eye

between 400 nm and 439 nm and 7% between 981 nm and 1100 nm. Since we are operating the detector to measure an optical flux which is in the order of 35 nW which is outside of the nominal power range for which the detector is calibrated (50 nW - 50 mW), we used the max value of 7% across the whole spectrum. The lamp intensity was measured and it appears to fluctuate by about 0.8% of its maximum intensity. However, if summed in quadrature with the uncertainty of the detector this contribution is negligible.

4 Optical absorbance

The optical absorbance is obtained from energy conservation:

$$1 = R_i(\lambda) + T_i(\lambda) + A_i(\lambda), \tag{2}$$

where R_i, T_i and A_i represent the reflectance, the transmittance and the absorbance for each film i, respectively. The resulting A_i curves are shown in Fig. 5 and the shaded areas represent the uncertainties.

Unlike the cases of transmittance (see Fig. 2) and reflectance (see Fig. 4), the spread between the different curves is much smaller and almost fully contained within the error bars. The inset of Fig. 5 shows the absorbance of the grAl films at 1100 nm as a function of the resistivity of the films. Any possible variation of absorbance with resistivity is within the measurement uncertainty of our setup.

In Fig. 6 we compare the average over all measured absorbance curves of our grAl films with other superconductors from the literature, with critical temperatures in the same range. We used a publicly available database of refractive indices for different materials and at different wavelengths produced by [27, 28] to obtain data on the transmittance and reflectance of thin films of Aluminum (Al), Molybdenum (Mo), Niobium (Nb), Titanium (Ti) and Titanium Nitride (TiN). The database provides easy ways to calculate both the reflectance and transmittance as a function of the wavelength, the angle of incidence (which was kept at 0°) and the thickness of the film (for further details see Appendix B.3). In order to compare with our grAl films, we fixed the thickness of all films to 20 nm.

MKIDs instruments that have been tested and deployed on sky such as DARKNESS [3] and MEC [4], use 60 nm thick films of PtSi as superconducting material with critical temperature in the range 0.8−1.0 K [9]. We therefore compare the absorption of our grAl films with the absorption of PtSi films. This comparison is not straightforward, as we need to compensate for different thicknesses; a thicker film absorbs more radiation than a thinner one. In a simplified picture, we assume that the reflectance of the material depends only on its surface and the transmittance decreases exponentially with the thickness of the film B.3.

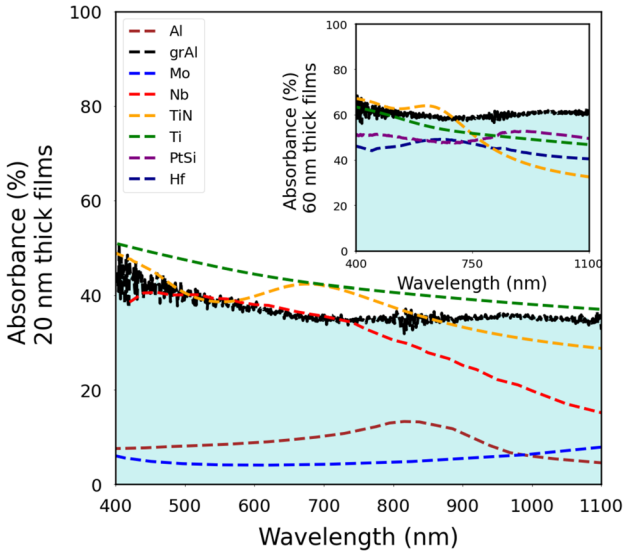

Fig. 6 Absorption of different 20 nm films of different superconductors commonly used in the MKIDs community: Brown - Aluminum, Blue - Molybdenum, Red - Niobium, Green - Titanium, Orange - Titanium Nitride (TiN). The black scatter represents the curve obtained by averaging the 5 curves of the grAl films shown in Fig. 5. The inset shows the absorption for selected materials including GrAl rescaled to be 60 nm thick. The PtSi (in Pink) value is taken from data published by [9], the Hf (in Dark Blue) is taken from data published by [8], all others are based on refractive index calculations

Increasing the thickness of the film three-fold results in a three-fold decrease in surface impedance, so that must be taken into account.

Figure 6 shows that 20 nm of grAl absorb about 40% of the impinging radiation across the whole 400 nm - 1100 nm band. Our data indicates that an MKID fabricated with a 20 nm thick film of grAl is as capable of absorbing visible and near infrared radiation with efficiencies similar to those of TiN MKIDs.

The inset of Fig. 6 shows a comparison between the extrapolated absorbance of GrAl, Ti and TiN, with measured PtSi data from [9]. We can infer that for 60 nm thick films, while the short-wavelength performance of Ti and TiN are marginally superior to grAl, grAl absorbs more visible and near-infrared radiation compared to PtSi films of the same thickness. Accordingly, it was estimated that a 90 nm thick film, if we imagined no reflectivity (e.g. by depositing anti-reflective coating on top of the film), would exhibit absorbance larger than 92% while retaining a large sheet inductance compared to other competing superconductors. Furthermore, being grAl deposited on sapphire substrates instead of silicon, it might exhibit better performance in terms of Two-Level Systems noise. A study on the TLS noise figure of grAl films can be found in [28]. It must be stated that the spectra can be treated with de-noising methods which are specific to thin film spectrometry [29] but were not used in this paper.

5 Conclusions

In an effort towards the development of better-performing MKIDs, we have carried out an investigation of the optical properties of grAl focusing on the reflectance and the absorbance of thin films of grAl of different morphology and consequently different resistivity, at room temperature. While reflectance and transmittance vary as the resistivity (i.e. the morphology) of the film varies, the absorbance appears to remain constrained within the uncertainties of our measurements. grAl is a promising superconductor for MKIDs because of its easy and affordable deposition, which yields uniform film thickness within $\pm$ 10%. We have shown that grAl films absorb light as efficiently as other - more technologically challenging - superconductors, already employed in the community such as PtSi and TiN, while offering higher sheet inductance and therefore prospects for device miniaturization in Megapixel-instruments. The study carried out for this report aims to produce a rough estimate of the optical properties of grAl films (thus indirectly inferring on n and k) based on simplified wave propagation models. Ellipsometry coupled with sophisticated dispersion models [30, 31], like Kramer-Kronig consistent methods, could offer a more comprehensive analysis and are intended for future work.

Appendix A Transmittance measurements

A.1 Error propagation

In order to calculate the errors on the transmittance curves, we have measured a data-stream of dark current from which we calculated the standard deviation and eventually, from the standard deviation, the peak-to-peak value and used this value to calculate the relative uncertainty on the current measured when measuring the photo-current when in front of the detector there is either the i-th grAl sample or a blank Sapphire wafer. The error on the transmittance figure was obtained by propagating such relative errors as described in [32].

$$\epsilon_{\text{peak-to-peak}} = 2.355 \times \sigma_{\text{dark-current}} \tag{3}$$

$$\epsilon_i = \epsilon_{\text{peak-to-peak}}/\text{grAl}_i \tag{4}$$

$$\epsilon_{Sapphire} = \epsilon_{\text{peak-to-peak}}/\text{Sapphire} \tag{5}$$

$$\epsilon_{Transmittance_i} = \sqrt{\epsilon^2_{grAl_i} + \epsilon^2_{Sapphire}} \times T_i \tag{6}$$

Appendix B Reflectance measurements

B.1 Measurement strategy

The reflectance measurement was carried out as follows:

First we measure the light reflected by the mirror ($I_{out,mirror}(\lambda)$) loaded in the sample holder, and by knowing its nominal reflectivity ($R_{mirror}(\lambda)$), we can calculate the impinging optical flux ($I_{in}(\lambda)$):

$$I_{out,\mathrm{mirror}}(\lambda) = R_{\mathrm{mirror}}(\lambda) \cdot I_{in}(\lambda) \tag{7}$$

Once we have calculated the impinging optical flux, and assuming we can neglect any fluctuation of the lamp intensity, we can now calculate the reflectivity of the sapphire wafer in a similar fashion:

$$I_{out}(\lambda) = \left[R_{\mathrm{Sapphire}}(\lambda) + o\left(T^2_{\mathrm{Sapphire}}\right)\right] \cdot I_{in}(\lambda) \tag{8}$$

Where R_{Sapphire} is the reflectance of the sapphire wafer, $o(T^2_{\{textSapphire}) = T_{\mathrm{Sapphire}} R_{\mathrm{Sapphire}} T_{\mathrm{Sapphire}} + ...$ includes any contribution due to multiple reflections in the sapphire. These are considered negligible due to the fact that $T^2_{\mathrm{Sapphire}} < 0.04$ across the whole wavelength range.

The samples we are characterizing consist of a thin grAl film deposited on a Sapphire substrate, therefore their reflectance depends mainly on the reflectance of the grAl film and on the reflectance of the Sapphire and the transmittance of the grAl films [33]. If we exclude higher-order effects such as multiple reflections, the reflectance of the stack can be calculated as:

$$I_{out}(\lambda) = I_{in}(\lambda) \cdot (R_i(\lambda) + T_i(\lambda) R_{\mathrm{Sapphire}}(\lambda) T_i(\lambda)) \tag{9}$$

Where, along with the already defined R_{Sapphire}, T_{Sapphire} and T_i, R_i represents the reflectance of the i-th grAl sample (see Table 1. The transmittance T_i when squared is < 0.16 and when multiplied by R_{Sapphire}, the second term in equation 9 as well as any other multiple-reflection effect contributes to at most 0.05. We have, therefore, neglected them in the calculation of the reflectance values shown in Fig. 4. We justify this assumption by the fact that the measured R_i are over an order of magnitude larger.

We noticed that the detector's reading was below the operating regime recommended by the manufacturer of 50 μW. This means that the calibration of the detector may need to be adjusted. In order to do that, we have characterized the reflectance of a blank sapphire wafer and compared it to literature estimates of 15% for normal incidence. We have therefore assumed that, for small variations in light intensity about the operating point, the response of the photodiode can be linearised. We have hence introduced a scaling factor that takes into account the corrections necessary to match the 15 % reflectance we expect from the sapphire substrate (our measurements lie at about 19–20%). We have also investigated if any reflection off the black cardboard could introduce any significant contribution to the measured signal. Our measurements indicate that if any contribution is present, it is below 0.5% and can therefore be neglected.

B.2 Error propagation

In order to calculate the errors on the transmittance curves, we have measured a data-stream of dark current from which we calculated the standard deviation and eventually, from the standard deviation, the peak-to-peak value and used this value to calculate the relative uncertainty on the current measured when measuring the photo-current when in front of the detector there is either the i-th grAl sample or a blank Sapphire wafer in a fashion that is entirely identical to what discussed in A.1. We have then noticed that the uncertainty quoted on the specs-sheet of the photodiode were larger than what we measured in this configuration. We were also operating the detector outside its nominal operation range, we have de thus decided, in a conservative fashion, to take maximum uncertainty quoted on the data-sheet (7%) and used it across the whole wavelength range. We have used a nominal (14%) uncertainty on the reflectance figure in order to account for both the uncertainty on the photo-current measured when the mirror and the photo-current measured when the grAl film is the optical path.

B.3 Calculation of absorption values from the database

The website http://www.refractiveindex.info is a database of simulated and experimentally measured values of optical constants. All data is derived from publicly available sources such as scientific journal articles and material data sheets published by manufacturers. In particular, a large number of datasets of real (n) and imaginary (k) refractive indices is available. At each wavelength value, the reflectance, which depends on material properties, is calculated from Fresnel's formulae [34] in their simplified form for perpendicular incidence:

$$R = \frac{(\mathbf{n}-1)^2}{(\mathbf{n}+1)^2} \tag{10}$$

Where $\mathbf{n}$ is a complex number $\mathbf{n} = n + ik$, and where we assume the refractive index of air to be 1. It is especially important to state that the Fresnel formulae only apply to simple interfaces and do not account for multiple interferences within the film.

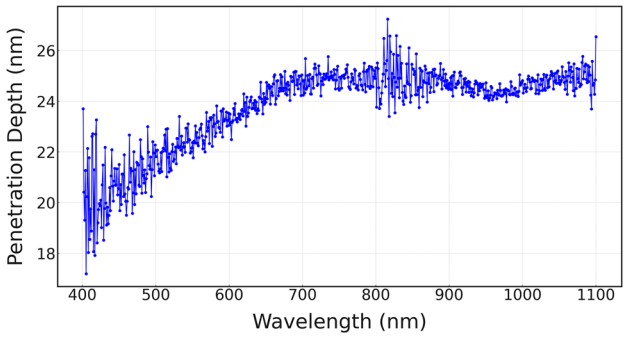

Fig. 7 Wavelength dependent penetration depth of VIS-NIR radiation as computed for grAl using data measured from 20nm thick films

In order to account for the losses inside the thin film, we have also calculated the absorption (α) of the material from its extinction coefficient (k) as follows:

$$\alpha = \frac{4\pi k}{\lambda} \tag{11}$$

with the obvious meaning of the symbols. Using the extinction coefficient, we have calculated the transmitted light in a film with thickness d as:

$$I(d) = I_0 e^{-\alpha d} \tag{12}$$

Consequently, the transmitted light can be evaluated as $I(d) = I_0(1 - e^{-\alpha d})$. The Beer-Lambert law (Eq. 12) is only valid in the case of a collimated beam and if we can neglect any internal effects in the film including interference.

For the sake of clarity, the penetration depth definied as the length in the material after which the intensity has decreased by a factor $1/e$, has been calculated and is shown in Fig. 7.

Acknowledgements The authors wish to thank the following funding bodies for support: Italian Space Agency under ASI Grants No. 2020-9-HH.0 and 2020-25-HH.0 (MDL). Science Foundation Ireland, under Grant No. 15/IA/2880 and 21/FFP-P/10213 (GU). This project has received funding from the European Union's Horizon 2020 research and innovation program under the Marie Skłodowska-Curie grant agreement number 847471 (QUSTEC) (MK, TR, IP). Furthermore, the authors want to thank Ben Mazin for providing the PtSi data shown in Fig. 6.

Author contributions MDL envisioned the experiments, conducted them and analysed the data, and wrote the initial draft of the manuscript. M.K and T.R fabricated the samples. I.P and G.U. contributed in the validation of the results. Everyone equally contributed to checking, editing and rewriting the final manuscript.

Funding This article is funded by Agenzia Spaziale Italiana (020-9-HH.0), Horizon 2020 Framework Programme (847471), Science Foundation Ireland (15/IA/2880).

Data availability The data that support the findings of this study are available from the corresponding author upon reasonable request.

Declarations

Conflict of interest The authors declare no competing interests.

References

1. G. Ulbricht, M. De Lucia, E. Baldwin, Applications for microwave kinetic induction detectors in advanced instrumentation. Appl. Sci. **11**(6), 2671 (2021). https://doi.org/10.3390/app11062671
2. B.A. Mazin, S.R. Meeker, M.J. Strader, P. Szypryt, D. Marsden, J.C. Eyken, G.E. Duggan, A.B. Walter, G. Ulbricht, M. Johnson et al., Arcons: a 2024 pixel optical through near-ir cryogenic imaging spectrophotometer. Publ. Astron. Soc. Pac. **125**(933), 1348–1361 (2013). https://doi.org/10.1086/674013
3. S.R. Meeker, B.A. Mazin, A.B. Walter, P. Strader, N. Fruitwala, C. Bockstiegel, P. Szypryt, G. Ulbricht, G. Coiffard, B. Bumble, G. Cancelo, T. Zmuda, K. Treptow, N. Wilcer, G. Collura, R. Dodkins, I. Lipartito, N. Zobrist, M. Bottom, J.C. Shelton, D. Mawet, J.C. Eyken, G. Vasisht, E. Serabyn, DARKNESS: a microwave kinetic inductance detector integral field spectrograph for high-contrast astronomy. Publ. Astron. Soc. Pac. **130**(988), 065001 (2018). https://doi.org/10.1088/1538-3873/aab5e7
4. A.B. Walter, N. Fruitwala, S. Steiger, J.I. Bailey, N. Zobrist, N. Swimmer, I. Lipartito, J.P. Smith, S.R. Meeker, C. Bockstiegel et al., The mkid exoplanet camera for subaru scexao. Publ. Astron. Soc. Pac. **132**(1018), 125005 (2020)
5. M. Dai, W. Guo, X. Liu, M. Zhang, Y. Wang, L. Wei, G. Hilton, J. Hubmayr, J. Ullom, J. Gao et al., Measurement of optical constants of tin and tin/ti/tin multilayer films for microwave kinetic inductance photon-number-resolving detectors. J. Low Temp. Phys. **194**, 361–369 (2019)
6. P. Szypryt, B.A. Mazin, G. Ulbricht, B. Bumble, S. Meeker, C. Bockstiegel, A. Walter, High quality factor platinum silicide microwave kinetic inductance detectors. Applied Physics Letters **109**(15), 1503–1511 (2016)
7. K. Kouwenhoven, I. Elwakil, J.V. Wingerden, V. Murugesan, D. Thoen, J. Baselmans, P.D. Visser, Model and measurements of an optical stack for broadband visible to near-infrared absorption in tin mkids. J. Low Temp. Phs. **209**(5), 1249–1257 (2022)
8. G. Coiffard, M. Daal, N. Zobrist, N. Swimmer, S. Steiger, B. Bumble, B. Mazin, Characterization of sputtered hafnium thin films for high quality factor microwave kinetic inductance detectors. Supercond. Sci. Technol. **33**(7), 07–02 (2020)
9. B. Mazin, J. Bailey, J. Bartlett, C. Bockstiegel, B. Bumble, G. Coiffard, T. Currie, M. Daal, K. Davis, R. Dodkins, N. Fruitwala, N. Jovanovic, I. Lipartito, J. Lozi, J. Males, D. Mawet, S. Meeker, K. O'Brien, M. Rich, J. Smith, S. Steiger, N. Swimmer, A. Walter, N. Zobrist, J. Zmuidzinas, Mkids in the 2020s. Bulletin of the AAS **51**(7) (2019). https://baas.aas.org/pub/2020n7i017. 27 Sept 2024
10. R.W. Cohen, B. Abeles, Superconductivity in granular aluminum films. Phys. Rev. **168**, 444–450 (1968). https://doi.org/10.1103/PhysRev.168.444
11. G. Deutscher, M. Gershenson, E. Grünbaum, Y. Imry, Granular superconducting films. J. Vac. Sci. Technol. **10**(5), 697–701 (1973). https://doi.org/10.1116/1.1318416
12. N. Maleeva, L. Grünhaupt, T. Klein, F. Levy-Bertrand, O. Dupre, M. Calvo, F. Valenti, P. Winkel, F. Friedrich, W. Wernsdorfer et al., Circuit quantum electrodynamics of granular aluminum resonators. Nat. Commun. **9**(1), 3889 (2018)
13. F. Levy-Bertrand, T. Klein, T. Grenet, O. Dupré, A. Benoît, A. Bideaud, O. Bourrion, M. Calvo, A. Catalano, A. Gomez et al., Electrodynamics of granular aluminum from superconductor to

insulator: observation of collective superconducting modes. Phys. Rev. B (2019). https://doi.org/10.1103/physrevb.99.094506
14. L. Sun, L. DiCarlo, M.D. Reed, G. Catelani, L.S. Bishop, D.I. Schuster, B.R. Johnson, G.A. Yang, L. Frunzio, L. Glazman, M.H. Devoret, R.J. Schoelkopf, Measurements of quasiparticle tunneling dynamics in a band-gap-engineered transmon qubit. Phys. Rev. Lett. **108**, 230509 (2012). https://doi.org/10.1103/PhysRevLett.108.230509
15. H. Rotzinger, S.T. Skacel, M. Pfirrmann, J.N. Voss, J. Münzberg, S. Probst, P. Bushev, M.P. Weides, A.V. Ustinov, J.E. Mooij, Aluminium-oxide wires for superconducting high kinetic inductance circuits. Supercond. Sci. Technol. **30**(2), 025002 (2016). https://doi.org/10.1088/0953-2048/30/2/025002
16. L. Grünhaupt, N. Maleeva, S.T. Skacel, M. Calvo, F. Levy-Bertrand, A.V. Ustinov, H. Rotzinger, A. Monfardini, G. Catelani, I.M. Pop, Loss mechanisms and quasiparticle dynamics in superconducting microwave resonators made of thin-film granular aluminum. Phys. Rev. Lett. (2018). https://doi.org/10.1103/physrevlett.121.117001
17. P. Kamenov, W.-S. Lu, K. Kalashnikov, T. DiNapoli, M.T. Bell, M.E. Gershenson, Granular aluminum meandered superinductors for quantum circuits (2019)
18. L. Grünhaupt, M. Spiecker, D. Gusenkova, N. Maleeva, S.T. Skacel, I. Takmakov, F. Valenti, P. Winkel, H. Rotzinger, W. Wernsdorfer et al., Granular aluminium as a superconducting material for high-impedance quantum circuits. Nat. Mater. **18**(8), 816–819 (2019)
19. P. Winkel, K. Borisov, L. Grünhaupt, D. Rieger, M. Spiecker, F. Valenti, A.V. Ustinov, W. Wernsdorfer, I.M. Pop, Implementation of a Transmon Qubit Using Superconducting Granular Aluminum. Phys. Rev. X **10**(3), 031032 (2020). https://doi.org/10.1103/PhysRevX.10.031032
20. V. Gupta, P. Winkel, N. Thakur, P. Vlaanderen, Y. Wang, S. Ganjam, L. Frunzio, R.J. Schoelkopf, Low loss lumped-element inductors made from granular aluminum. arXiv preprint arXiv:2411.12611 (2024). 27 Sept 2024
21. F. Levy-Bertrand, A. Benoît, O. Bourrion, M. Calvo, A. Catalano, J. Goupy, F. Valenti, N. Maleeva, L. Grünhaupt, I.M. Pop, A. Monfardini, Subgap kinetic inductance detector sensitive to 85-GHz radiation. Phys. Rev. Appl. **15**(4), 044002 (2021). https://doi.org/10.1103/PhysRevApplied.15.044002
22. F. Valenti, F. Henriques, G. Catelani, N. Maleeva, L. Grünhaupt, U. Lüpke, S.T. Skacel, P. Winkel, A. Bilmes, A.V. Ustinov, J. Goupy, M. Calvo, A. Benoît, F. Levy-Bertrand, A. Monfardini, I.M. Pop, Interplay between kinetic inductance, nonlinearity, and quasiparticle dynamics in granular aluminum microwave kinetic inductance detectors. Phys. Rev. Appl. **11**(5), 054087 (2019). https://doi.org/10.1103/PhysRevApplied.11.054087
23. H. Monard, F. Sabary, Optical properties of silver, gold and aluminum ultra-thin granular films evaporated on oxidized aluminum. Thin Solid Films **310**(1–2), 265–273 (1997)
24. K. Borisov, D. Rieger, P. Winkel, F. Henriques, F. Valenti, A. Ionita, M. Wessbecher, M. Spiecker, D. Gusenkova, I.M. Pop, W. Wernsdorfer, Superconducting granular aluminum resonators resilient to magnetic fields up to 1 Tesla. Appl. Phys. Lett. **117**(12), 120502 (2020). https://doi.org/10.1063/5.0018012
25. A.G. Moshe, E. Farber, G. Deutscher, Optical conductivity of granular aluminum films near the mott metal-to-insulator transition. Phys. Rev. B **99**(22), 224503 (2019)
26. M. Ballester, E. Marquez, J. Bass, C. Würsch, F. Willomitzer, A.K. Katsaggelos, Review and novel formulae for transmittance and reflectance of wedged thin films on absorbing substrates. Meas. Sci. Technol. **36**(2), 025502 (2025)
27. M. Polyanskiy, refractiveindex.info: A database of optical constants. figshare (2024). https://doi.org/10.6084/m9.figshare.c.6868000.v1. https://springernature.figshare.com/collections/refractiveindex_info_A_database_of_optical_constants/6868000/1. 27 Sept 2024
28. M. Kristen, J. Voss, M. Wildermuth, A. Bilmes, J. Lisenfeld, H. Rotzinger, A. Ustinov, Giant two-level systems in a granular superconductor. Phys. Rev. Lett. **132**(21), 217002 (2024)
29. D. Minkov, G. Angelov, D. Nikolov, R. Rusev, E. Marquez, S. Fernandez, Method for superior denoising of uv/vis/nir transmittance spectra of thin films. Opt. Express **32**(19), 33758–33778 (2024)
30. D.V. Likhachev, N. Malkova, L. Poslavsky, Modified tauc-lorentz dispersion model leading to a more accurate representation of absorption features below the bandgap. Thin Solid Films **589**, 844–851 (2015)
31. S. Wemple, M. DiDomenico Jr., Behavior of the electronic dielectric constant in covalent and ionic materials. Phys. Rev. B **3**(4), 1338 (1971)
32. J.R. Taylor, An Introduction to Error Analysis: The Study of Uncertainties in Physical Measurements. ASMSU/Spartans.4.Spartans Textbook. University Science Books, (1997). https://books.google.it/books?id=ypNnQgAACAAJ. 27 Sept 2024
33. B. Hapke, Bidirectional reflectance spectroscopy: 1. Theory. J. Geophys. Res.: Solid Earth **86**(B4), 3039–3054 (1981)
34. M. Born, E. Wolf, *Principles of Optics: Electromagnetic Theory of Propagation, Interference and Diffraction of Light* (Elsevier, Amsterdam, 2013)
35. G. Deutscher, H. Fenichel, M. Gershenson, E. Grünbaum, Z. Ovadyahu, Transition to zero dimensionality in granular aluminum superconducting films. J. Low Temp. Phys. **10**, 231–243 (1973)